Journal of the European Ceramic Society **10** (1992) 381–392

Redistribution of Ce and La during Processing of Ce(La)-TZP/Al_2O_3 Composites

Herbert K. Schmid, R. Pennefather

Division of Materials Science and Technology, CSIR, PO Box 395, Pretoria 0001, South Africa

S. Meriani & C. Schmid

Instituto di Chimica Applicata ed Industriale, University of Trieste, Italy

(Received 24 October 1991; accepted 10 January 1992)

Abstract

The dispersion of second-phase particles, platelets or fibres in a ceramic body offers possibilities of considerable improvements in mechanical properties. In such second-phase reinforced composites the materials properties are to a large extent controlled by the structure of the internal interfaces, i.e. the phase and grain boundaries.

The microstructure/microchemistry of alumina-dispersed ceria-stabilized tetragonal zirconia polycrystals (Ce-TZP/20A) were characterized by means of analytical TEM/STEM techniques. Local variation in the concentration of Ce stabilizer as well as of La additives and Si impurities during processing of the composite ceramics were studied by EDS X-ray analysis with high spatial resolution. Emphasis was put on the segregation of Ce and La in interface regions. Evidence was found for the presence of a vitreous intergranular phase situated in small pockets at triple grain junctions. The addition of small fractions of La_2O_3 in TZP resulted in interreaction between matrix constituents and Al_2O_3 particles. In this reaction a stable crystalline Al–Ce–La–Zr mixed oxide phase is formed, effectively reducing the fraction of residual vitreous intergranular phase, resulting in improved fracture toughness in this material.

Die Dispersion sekundärer Teilchen, Plättchen oder Fasern in einem Keramikkörper bietet Möglichkeiten, die mechanischen Eigenschaften beträchtlich zu verbessern. In solchen durch Sekundärphasen verstärkten Verbundwerkstoffen werden die Materialeigenschaften weitgehend durch die Struktur der inneren Granzflächen, d.h. Phasen- und Korngrenzen, bestimmt.

Die Mikrostruktur/Mikrochemie von Alumina-dispergierten Ceria-stabilisierten polykristallinen Zirkoniakeramiken (Ce-TZP/20A) wurden mittels analytischen TEM/STEM-Techniken charakterisiert. Lokale Änderungen in der Ce-Konzentration wie auch von La-Zusätzen und Si-Verunreinigungen während der Herstellung der Verbundkeramiken wurden durch EDS-Röntgenanalyse mit hoher räumlicher Auflösung untersucht. Besondere Aufmerksamkeit wurde auf die Segregation von Ce und La in den Bereichen der inneren Grenzflächen gerichtet. Die Präsenz einer glasartigen intergranularen Phase in kleinen Zwickeln an Korngrenztripelpunkten konnte nachgewiesen werden. Der Zusatz von La_2O_3 in geringen Anteilen in TZP bewirkte eine Interreaktion zwischen Matrixelementen und Alumina-Teilchen. In dieser Reaktion wird eine stabile kristalline Al–Ce–La–Zr Mischoxidphase gebildet, wodurch sich der Anteil der verbleibenden intergranularen Glasphase effektiv verringert, mit dem Ergebnis einer verbesserten Bruchzähigkeit in diesem Material.

La dispersion de particules d'une seconde phase comme des platelets ou des fibres dans une céramique, offre des possibilités d'améliorer de façon considérable les propriétés mécaniques. Dans de tels composites renforcés par une seconde phase, les propriétés du matériau sont pour une grande part contrôlées par la structure des interfaces internes, c'est à dire de la phase et des joints de grains.

La microstructure/microchimie de polycristaux de

Journal of the European Ceramic Society 0955-2219/92/$5.00

zircone tetragonale contenant de l'alumine dispersée et stabilisée par de la cérine (Ce-TZP/20A) ont été caractérisées au moyen des techniques analytiques TEM/STEM. Des variations locales de la concentration en stabilisateur Ce ainsi que des additifs à base de La et des impuretés de Si durant l'obtention des céramiques composites ont été étudiées par analyse EDX-RX avec une haute résolution spatiale. L'accent a été mis sur la ségrégation de Ce et La dans les régions interfaciales. La présence d'une phase vitreuse intergranulaire située dans des petites poches aux jonctions triples entre grains a été mise en évidence. De l'addition de petites fractions de La_2O_3 dans TZP a résulté une réaction entre les constituants de la matrice et les particules d'Al_2O_3. Par cette réaction une phase composée d'un mélange d'oxides d'Al–Ce–La–Zr s'est formée, réduisant de façon effective la fraction en phase vitreuse intergranulaire résiduelle, et ainsi améliorant la résistance à la fracture de ce matériau.

1 Introduction

Tetragonal ZrO_2 polycrystals (TZP) are of considerable interest for advanced structural applications because of their exceptionally good combination of mechanical properties and remarkable transformation plasticity behaviour.[1-4] However, often limitations occur for high-temperature applications due to the presence of residual intergranular phases that result from liquid-phase sintering with oxide additions. The most commonly used additives, Y_2O_3 and CeO_2, which form solid solutions with ZrO_2 and thus stabilize its tetragonal symmetry, also effectively assist in densification during sintering of TZP. However, these additives tend to form vitreous intergranular phases together with impurities segregated to grain boundaries,[1,5,6] resulting in a degradation of high-temperature properties, particularly bending strength and creep behaviour.

Considerable efforts have been made during recent years to overcome the shortfalls of monolithic ceramics, i.e. their inherently low fracture toughness and declining strength at elevated temperature, by the dispersion of second-phase particles, platelets or fibres in a ceramic body (ceramic matrix composite, CMC).[7,8] Improvements in bending strength and fracture toughness up to $\sigma = 2400$ MPa (three-point bending strength) and $K_{IC} = 17\,\text{MPa}\,\text{m}^{1/2}$ (critical stress intensity factor measured in four-point bending of chevron-notched beams), respectively have been reported for zirconia/alumina composites.[9,10] The beneficial effects of second-phase Al_2O_3 particles dispersed in a TZP matrix are (i) effective control of grain growth[11,12] thus enabling the optimization of the microstructure, and (ii) toughening by microcracking and crack deflection.[8,13]

Understanding the segregation behaviour of Ce and La dopants and their role in the interreaction between matrix constituents and alumina particles is of importance for the optimization of Ce(La)-TZP/Al_2O_3 composites. Hence detailed investigations on the structure of interfaces, involving structural and microchemical analysis with high spatial resolution by means of analytical transmission electron microscopy (AEM) are required. Studies on the microstructural evolution as a result of reactions taking place at the internal interfaces during heat treatment permit a mechanical property correlation and thus the tailoring of materials having specific properties through the control of these processes. In the present work, two CeO_2-stabilized tetragonal ZrO_2/alumina composites were prepared and their resulting microstructure/microchemistry were characterized by AEM techniques. In these studies the influence of La_2O_3 on phase interreaction is identified. Emphasis is put on the redistribution of Ce and La additives and their role in the formation of residual intergranular phases during processing of these composite ceramics.

2 Experimental Procedure

Two zirconia/alumina composite ceramics with nominal chemical composition (in mol% of total composition) 9·0 CeO_2 + 66·7 ZrO_2 + 24·3 Al_2O_3 (composite CZA), and 8·3 CeO_2 + 0·7 La_2O_3 + 66·7 ZrO_2 + 24·3 Al_2O_3 (composite CLZA) were prepared by the mixed oxide route. CeO_2-Stabilized tetragonal zirconia polycrystals, 12Ce-TZP, and 11Ce(1La)-TZP, respectively, were mixed with 20 wt% Al_2O_3 by attrition milling for 3 h in isopropanol using ZrO_2 beads as milling media. The respective weight fractions of the constituents are listed in Table 1. Disc-shaped green compacts (5 mm × 10 mm in diameter) were produced by cold isostatic pressing the powder mixtures at 200 MPa. The green compacts were sintered at 1400°C for 4·5 h; maximum heating rate was 400°C/h.

In order to understand the chemical changes associated with the microstructural evolution during the processing of Ce(La)-TZP/Al_2O_3 composites, Ce and La distributions were analysed in these two systems by means of analytical TEM. Thin electron-

Table 1. Sample material preparation and properties

	Composition (wt%)				*Properties*[a]				*Phases*[b] *detected*
	Al_2O_3	CeO_2	La_2O_3	ZrO_2	ρ	H_v	σ	K_{IC}	
12Ce-TZP/20A (composite CZA)	20	12·8	—	67·2	97·9	11·0	600	12·2	CZ, A, V
11Ce (1La)-TZP/20A (composite CLZA)	20	11·6	1·9	66·5	96·8	11·7	493	15·5	CZ, A, M, V

[a] ρ, % theoretical density; H_v, Vickers hardness (GPa); σ, flexural strength (four-point bending) (MPa); K_{IC}, fracture toughness (critical stress intensity factor measured by chevron-notched beam technique) (MPa $m^{1/2}$).
[b] CZ, Ce-TZP matrix; A, Al_2O_3 phase; M, mixed phase (Ce, La, Zr, oxide); $12Al_2O_3$; V, vitreous intergranular phase.

transparent foils were prepared by cutting the sintered compacts into 120-μm thick slices using a diamond wafering saw. Discs 3 mm in diameter were further thinned by dimple grinding and polishing to a thickness $t \approx 15\,\mu$m, followed by ion milling (5 kV Ar ions, 12° angle of incidence). The foils were coated with a thin film of amorphous carbon to avoid electrical charging. The samples were examined in an analytical scanning transmission electron microscope (STEM) operated at an accelerating voltage of 120 kV (Philips EM 420 analytical STEM wth EDAX PV 9900 EDS and GATAN 607 EELS attachments). The instrument was equipped with energy-dispersive X-ray spectrometer (EDS) and electron energy-loss spectrometer (EELS) attachments for chemical microanalysis. In EDS microanalysis a spatial resolution in the order of 5 nm was achieved by condensing the electron beam to a fine probe having an effective spot size of 3 nm in STEM mode and taking spherical aberration effects of the second condenser lens as well as beam spreading in a Ce-TZP foil of thickness $t \approx 35$ nm into account.[14] Under these conditions it was possible to analyse the composition of the intergranular phase situated in small pockets at triple gain junctions with a tolerable phase overlap error $\leq 25\%$ (relative). However, due to inherently low beam intensities and low X-ray yield for light elements, the statistical error in single measurements can be considerably high, especially for elements present in small concentrations, yielding counting errors of the order of $\approx 20\%$ (for Si), $\approx 15\%$ (La) and $\approx 10\%$ (Ce), respectively. Since count times usefully cannot exceed 400 s because of specimen contamination when the electron probe is condensed to a small spot, the statistical error is effectively reduced by adopting the multiple-spectra method[15] for quantitative phase analysis. Whenever possible, 15 to 20 spectra of individual grains were collected by means of a (semi)-autoanalysis routine (EDAX PV CHEM Software Package for automated EDS analysis in STEM) and statistically evaluated. The autoanalysis mode provides for automated multi-point EDS analysis in STEM and proved to be also extremely useful for the investigation of solute segregation to internal interfaces by measuring composition profiles by spot-by-spot analysis across interfaces.[16]

Relative concentrations of Al, La, Ce and Zr constituents as well as Si impurities were estimated from the integrated intensity ratios of the AlK SiK, ZrK, LaL and CeL lines using calculated values for the (Cliff-Lorimer) K_{AB} factors in the standardless thin film approximation. Relatively large fit errors arise in the quantitation of La and Si because of considerable peak overlap of the LaL, CeL and SiK, ZrL lines, as well as uncertainties in the background modelling in the energy region $E < 2$ keV. The accuracy of the peak deconvolution critically depends on the energy calibration of the EDS system. Hence the estimated total uncertainty in the quantification of La and Si has to be put in the order of 20%, whereas for the other constituents a relative error $< 10\%$ could be achieved in phase analysis.

3 Results

3.1 Microstructure of 12Ce-TZP/20A (composite CZA)

The microstructure and microchemistry of phase and grain boundary areas in alumina-dispersed zirconia composite ceramics have been investigated by means of conventional transmission electron microscopy (CTEM) and analytical scanning transmission electron microscopy (AEM/STEM). The micrograph in Fig. 1 shows the STEM image (mixed transmitted electron bright field (BF) and secondary electron (SE) signals) of Al_2O_3 particles (A) dispersed in the Ce-TZP matrix (CZ). The larger A particles, of mean size around 0·5 μm, show convexly curved as well as faceted surfaces and are intergranularly dispersed within the CZ matrix. Measurements of the linear intercept in SEM images indicated a mean size GS $\approx 1\,\mu$m for the CZ matrix grains. Occasionally, smaller spherical A particles, 25 to 200 nm in diameter, have been observed in

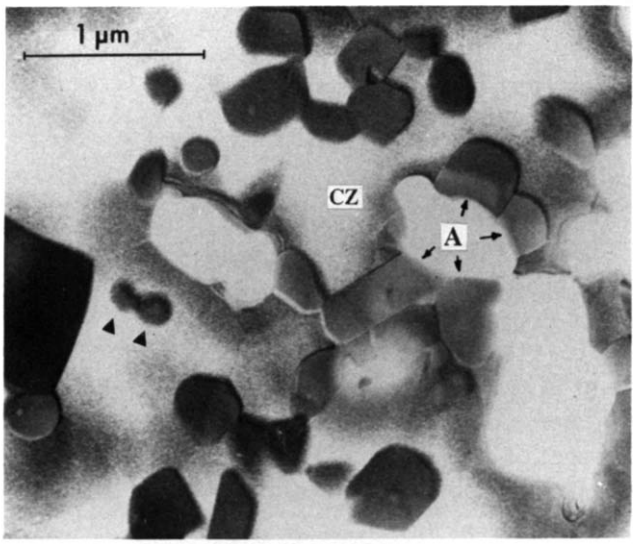

Fig. 1. Microstructure of composite CZA: STEM (BF + SE signals) image showing Al_2O_3 particles (A) dispersed in Ce-TZP matrix (CZ); small spherical particles in intragranular positions are marked by arrows.

intragranular positions inside CZ grains (marked by arrows). The observation of misfit dislocations in phase and grain boundaries in this material, indicating an essentially crystalline nature of these interfaces and a non-continuous intergranular phase restricted to pockets at multiple grain junctions, was reported in previous investigations.[17] The existence of a vitreous intergranular phase situated in small pockets at triple grain junctions (TJ) was revealed by CTEM imaging at high magnification (Figs 2(a) and 3(a)). At mixed alumina–zirconia–alumina type triple grain junctions (AZA-TJ), often wedge-shaped salients of the CZ matrix extending into regions between the A grains have been observed (Fig. 3(a)). The diffraction contrast in CTEM images indicates a crystalline nature for such salient regions.

3.2 EDS microanalysis in composite CZA

Local variation in chemical composition was analysed with high spatial resolution by means of

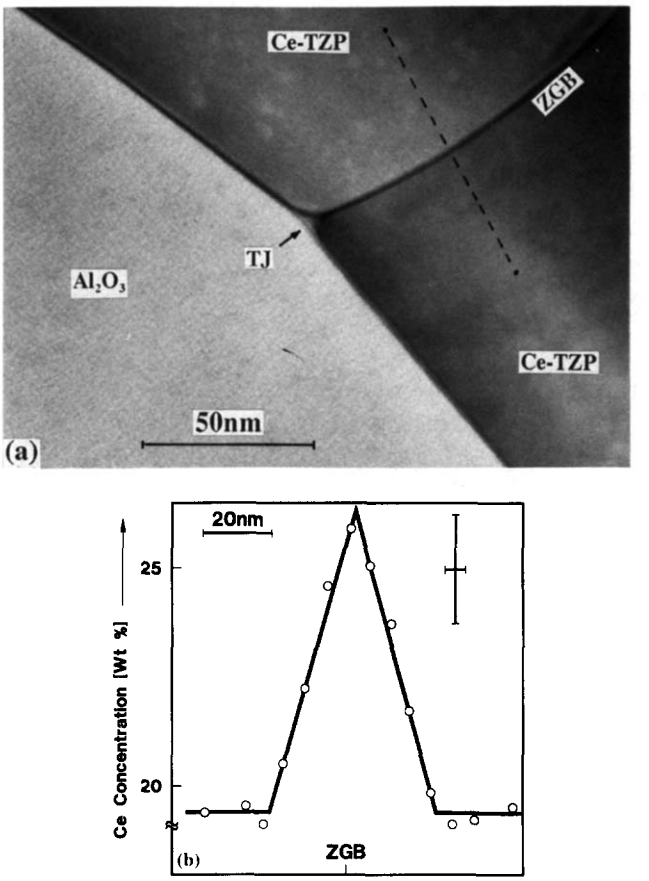

Fig. 2. Structure of phase and grain boundaries in composite CZA: (a) CTEM (BF) image reveals the presence of residual intergranular phase in pocket at triple grain junction (TJ); (b) Ce concentration profile across grain boundary in Ce-TZP matrix (ZGB).

standardless quantitative EDS analysis in STEM. The results of the X-ray analysis of CZ and Al_2O_3 constituent phases as well as residual intergranular phases in the composite CZA are presented in Table 2. Relative concentrations are listed in wt% cations normalized to 100%. The concentrations listed for the constituent phases are the result of 15 individual spectra which were evaluated statistically at the 95% confidence level. The analysis of the CZ matrix revealed (i) the presence of Si impurities, (ii) a Ce

Table 2. EDS analysis in 12 Ce-TZP/20A (composite CZA)

Phase	*Concentration (wt% cations)*			
	Al	*Si*	*Ce*	*Zr*
12Ce-TZP (nominal)	—	—	17·3	82·7
CZ matrix	<0·5	2	19·5 (±1·5)	78
Al_2O_3 grain	>98·6	—	—	<1·3
Matrix TJ (1)[a]	—	2·5	25	72
AZA-TJ (2)[a]	30	4	46	20

[a] Averaged value of 10 measurements on intergranular glassy phase in small pockets at (1) CZ matrix triple grain junctions, (2) mixed alumina–zirconia–alumina triple grain junctions.

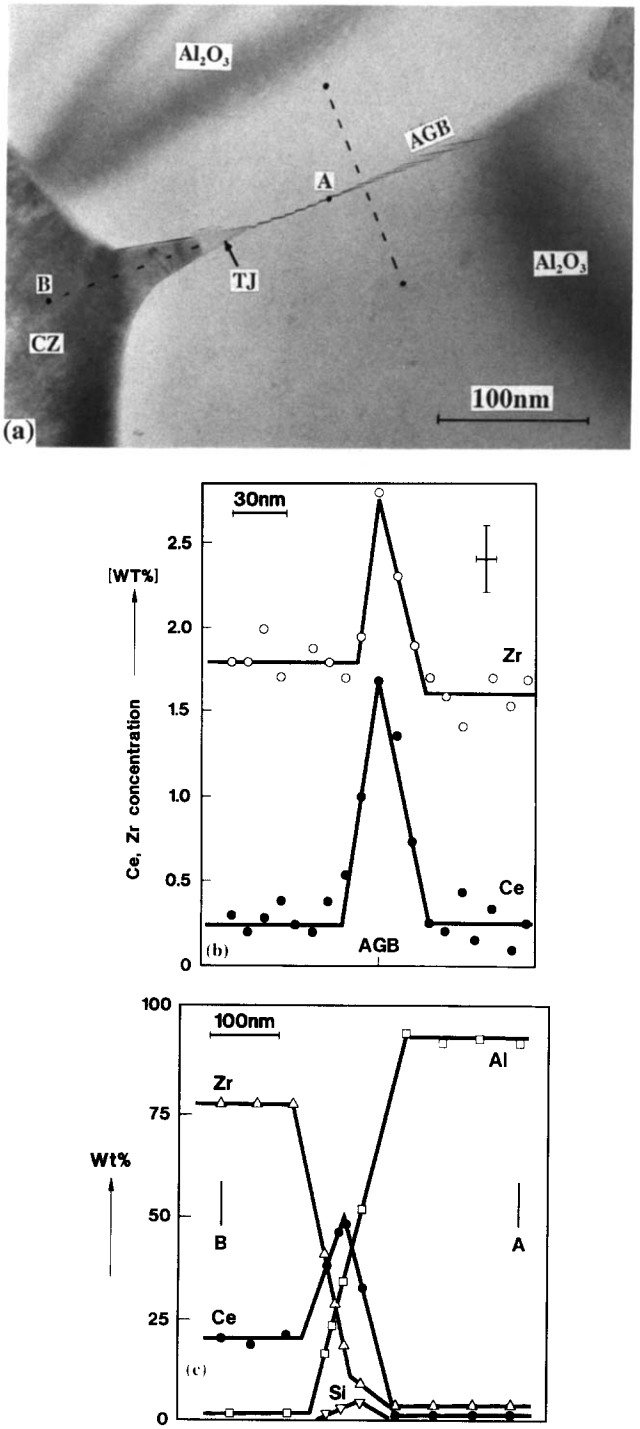

Fig. 3. Structure and chemistry of interfaces in CZA: (a) TEM-BF showing wedge-shaped salient formed in CZ matrix in mixed alumina–CZ–alumina triple grain junction area; (b) composition profiles across alumina grain boundary (AGB); (c) composition profiles along the line A–B (as indicated in (a)).

concentration slightly above the nominal value, and (iii) a marginal Al concentration close to the detection limit of the EDS system employed. To avoid phase overlap conditions, grains having hexagonal cross-sections with diameters well exceeding the foil thickness were chosen for analysis. The EDS results indicated a purity in excess of 98% Al_2O_3 content for the A particles analysed.

The multiple-spectra approach cannot be applied to the analysis of small pockets of intergranular phase and to the measurement of composition profiles across phase and grain boundaries. Though the composition of intergranular phase showed considerable variation from measurement to measurement, which reflects the degree of inhomogeneity in the glass phase, trends can be verified with confidence by comparison of analysis results measured on a large number of individual triple grain junctions. The EDS results indicate Si and Ce enrichment in the vitreous intergranular phase in pockets at matrix TJs and considerable Al and Ce enrichment in pockets at mixed AZA-TJs.

Composition profiles were measured by automated spot-by-spot EDS analysis (spot size ≈ 3 nm) across grain boundaries in the CZ matrix (ZGB, Fig. 2(b)), and across alumina grain boundaries (AGB, Fig. 3(b)). The positions of the line scans are indicated in Fig. 2(a) and Fig. 3(a), respectively. Uncertainties in the Ce and Zr concentration as well as in the lateral positioning of the electron probe (with respect to the interface) are indicated by error bars. Although uncertainties in the relative concentrations are high in individual single analysis points, the results clearly revealed a pronounced Ce segregation at matrix grain boundaries (ZGB), as well as Ce and Zr segregation at alumina grain boundaries (AGB). Composition profiles across the CZ/A phase boundaries (ZAPB) along the line A–B in the CZ salient region (Fig. 3(a)) indicate a considerable Ce enrichment at the tip of the salient; Si impurities levels also showed a marked increase in this TJ region (Fig. 3(c)).

3.3 Microstructure of 11Ce(1La)-TZP/20A (composite CLZA)

The characteristic microstructural features as observed in composite CLZA are depicted in the CTEM micrograph in Fig. 4(a). The Ce-TZP matrix (CZ) is in coexistence with an Al–Ce–La–Zr mixed oxide phase (M phase) and pure Al_2O_3 (A phase). Mean grain sizes in the order of 1 μm were observed for both the M and A phase and GS $\approx 1{\cdot}7$ μm for the CZ matrix. Though TEM 'diffuse' dark field (DF) images indicate that there is very little residual glass phase present in the composite CLZA, high magnification images revealed the existence of vitreous intergranular phase in very small pockets at TJs (Fig. 4(b)). Occasionally, macrocracks had developed in thin foils during specimen preparation. The fracture surfaces observed in TEM micrographs revealed a preference for transgranular fracture (e.g. grain GR I, Fig. 5(a)).

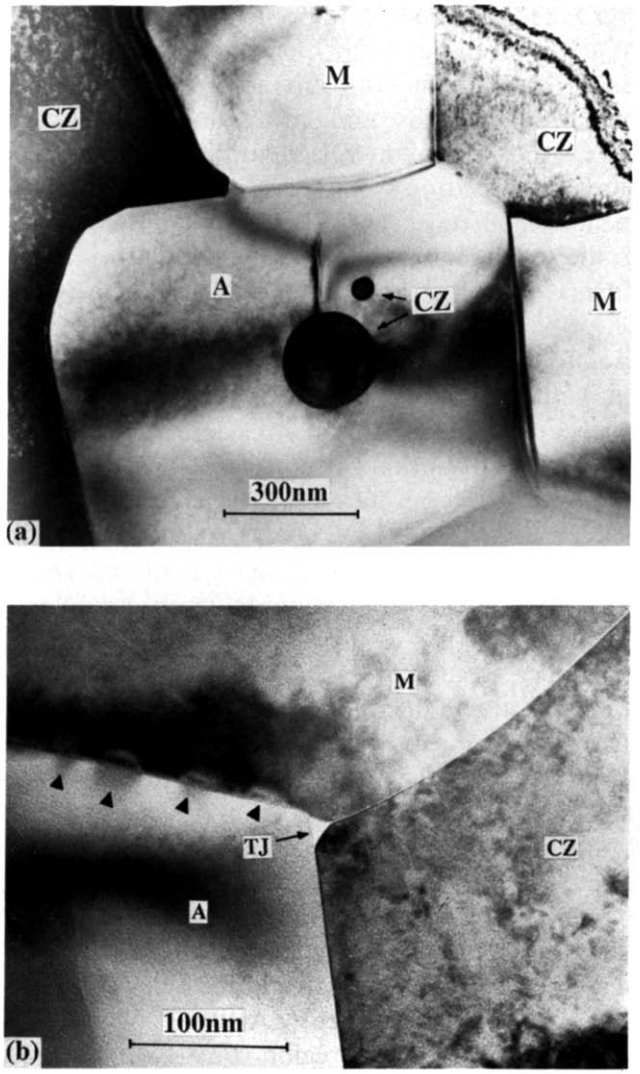

Fig. 4. Microstructure of composite CLZA: (a) TEM-BF showing CZ matrix in coexistence with alumina (A) and Al–Ce–La–Zr mixed oxide phase M; (b) residual intergranular phase in pocket at mixed A–CZ–M triple grain junction (CTEM-BF); strain contrasts at A–M phase boundary are marked by arrows.

The surfaces of M grains were observed to be either convexly curved (e.g. ZMPB, Figs 4(b), 5(a)), or faceted as seen in lattice fringe images (Fig. 6(a)). Indexing of electron diffraction patterns taken from M grains is compatible with a crystal structure of hexagonal symmetry and lattice parameters $a = 0{\cdot}56$ nm, $c = 2{\cdot}20$ nm.

Occasionally, grains of an unidentified (Ce, La)-rich crystalline phase (Fig. 5(a), GR III) were observed in coexistence with the CZ matrix and the M phase. Though the exact crystal structure of this phase has not yet been established, precision measurements on the chemical shift of the Ce-$M_{4,5}$ ionization edges in EEL spectra indicated that Ce ions in both the M phase as well as in this unknown (Ce, La)-rich phase are partially reduced to their trivalent Ce^{3+} state.[18]

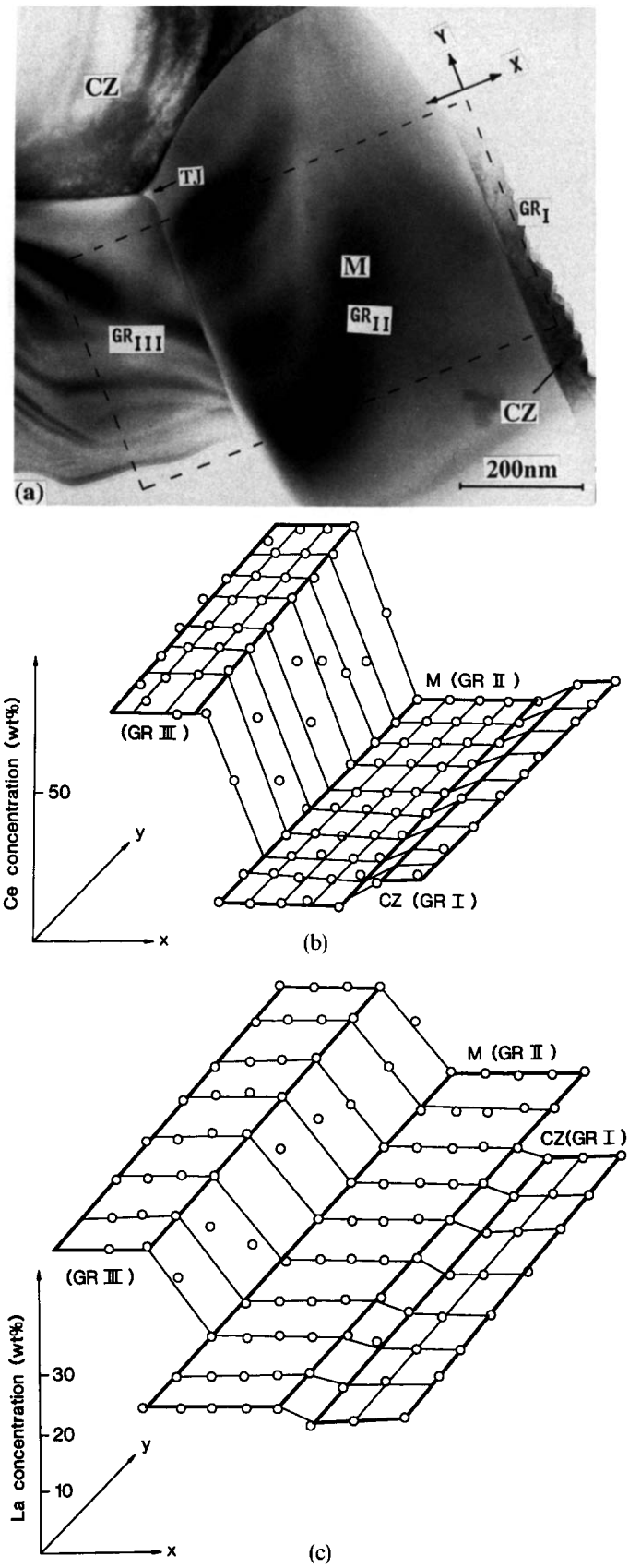

Fig. 5. Microstructure of composite CLZA: (a) CTEM micrograph showing M phase (GR II) in coexistence with (Ce, La)-rich grain (GR III). 10 × 12 matrix points were analysed by EDS autoanalysis in STEM within the framed area. Schematic representation of (b) Ce concentration and (c) La concentration as a function of x,y-coordinates within the framed area.

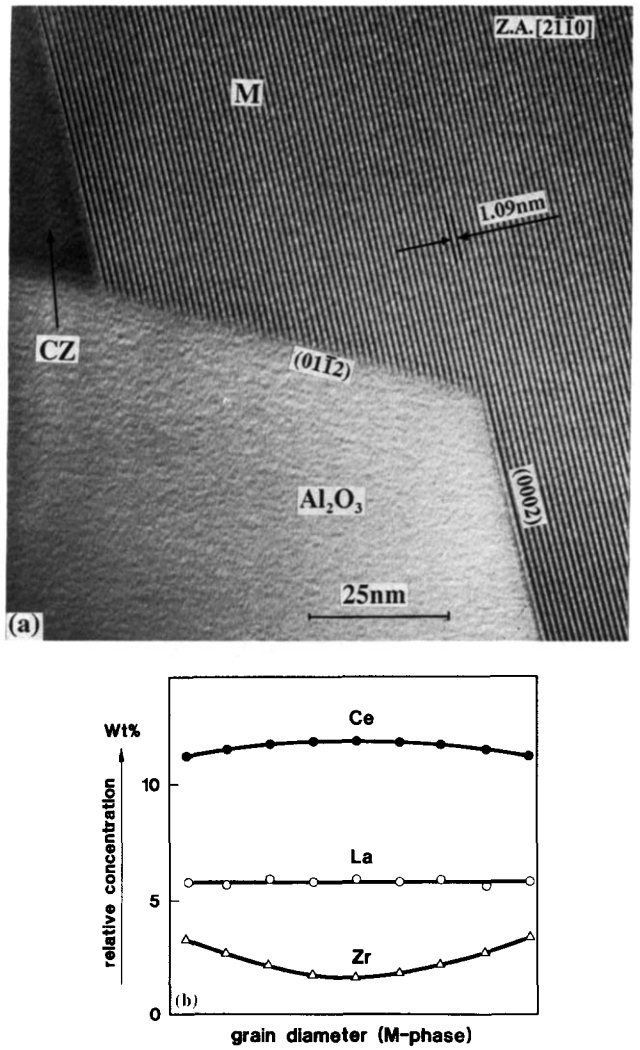

Fig. 6. Structure and chemistry of M phase: (a) Lattice fringe image of M grain shows faceting of grain surfaces; (b) composition gradients across M grain.

3.4 EDS microanalysis in composite CLZA

Results of the X-ray analysis in composite CLZA are presented in Table 3, along with standard deviations of the multiple-spectra analysis (in parentheses). The analysis revealed the coexistence of three principal phases: (i) the CZ matrix having identical chemical composition (within the limits of measuring errors) as in the composite CZA; little or no La was detected in all CZ matrix grains analysed; (ii) a crystalline Al–Ce–La–Zr mixed oxide phase (M); and (iii) pure Al_2O_3. Occasionally observed spherical inclusions confined in Al_2O_3 grains have been identified as pure CZ phase showing no indication of interreaction. Spot analysis at triple grain junctions (TJs) revealed Si, Al and La enrichment in the vitreous intergranular phase present in very small pockets at TJs.

A full 10 (lines) × 12 (points) matrix of analysis points was measured in STEM autoanalysis mode within the framed area indicated in Fig. 5(a). Results of this analysis are partially presented in Table 4 for relative La and Ce concentrations (in wt%), along with the mean concentration $\bar{C}(y)$ of each column (in y direction) and the standard deviation $S(y)$. Note the small standard deviations in columns 2 to 6 (GR II), which reflects the high homogeneity of the M phase. The concentrations C_{Ce} and C_{La} as function of coordinates x, y are shown schematically in a three-dimensional presentation in Fig. 5(b) and (c), respectively. Actually measured values for each matrix point are represented by open circles; the c coordinate of the overlaying grid is based on the mean concentration C in the respective phase areas. The application of the PV CHEM autoanalysis routine to a number of individual grains thus can generate a large number of data points which, statistically evaluated, allow the detection of composition gradients on levels far beyond the accuracy obtained in single measurements. Averaged Ce, La and Zr concentration gradients, as measured across 5 grains of the M phase, are shown in Fig. 6(b). The concentration gradients of Ce and Zr seem to be complementary, with maximum Ce and minimum Zr concentration measured in the centre of M grains. No indication of a gradient was detected for the La concentration.

As in composite CZA, composition profiles were measured across grain boundaries in the CZ matrix

Table 3. EDS analysis in 11Ce (1La)-TZP/20A (composite CLZA)

Phase	*Concentration (wt% cations)*				
	Al	*Si*	*La*	*Ce*	*Zr*
CZ (nominal)	—	—	2·9	15·7	81·4
CZ matrix	—	2	<0·7	19 (1·7)	78 (2·6)
Mixed phase M	76 (2·8)	—	8 (2·1)	13 (2·3)	3 (1·5)
Matrix TJ	4	5	4	22	65
AZM TJ[a]	70	15	2	5	8
GR III[b]	—	—	32	64	4

[a] Mixed M phase–alumina–CZ triple grain junction.
[b] (Ce, La)-rich phase, grain GR III Fig. 5(a).

Table 4. Multipoint EDS autoanalysis in composite CLZA (10 × 12 matrix, Fig. 5(a))

	Point number										
	GR I	*GR II*					*GR III*				
	1	*2*	*3*	*4*	*5*	*6*	*7*	*8*	*9*	*10*	*11*
						wt% La					
Line number											
5	—	5·7	5·8	5·6	5·7	6·5	11·0	31·8	31·5	31·1	30·2
6	2·0	5·1	5·5	5·9	6·1	6·2	27·2	31·5	32·7	30·9	30·4
7	3·0	5·6	5·4	6·1	5·3	6·1	24·1	30·4	32·4	31·8	29·8
8	5·1	6·1	5·7	5·8	5·9	6·4	18·0	32·4	32·2	31·7	30·4
9	9·3	6·0	6·2	5·3	5·8	6·0	17·2	31·5	31·5	31·4	30·6
10	4·1	6·3	4·8	6·2	5·9	6·2	22·0	31·5	31·7	31·7	33·2
$\bar{C}(y)$	—	5·80	5·57	5·82	5·78	6·23	—	31·52	32·00	31·43	30·53
$S(y)$	—	0·43	0·47	0·36	0·27	0·19	—	0·65	0·51	0·37	1·28
						wt% Ce					
Line number											
5	22·4	11·2	11·6	12·1	12·5	12·4	20·5	62·3	63·8	62·9	58·9
6	20·7	11·6	12·5	12·2	11·8	12·1	52·5	63·5	62·5	63·4	62·7
7	19·3	11·2	11·5	12·0	12·0	12·0	45·7	65·2	63·1	63·5	63·6
8	16·5	12·0	11·5	11·5	11·9	11·9	32·9	63·3	63·8	64·1	63·0
9	13·6	11·0	11·7	11·7	11·6	11·2	31·0	64.7	64·6	64·9	62·9
10	10·6	10·6	10·8	11·2	11·4	11·8	38·8	65·2	64·3	64·2	59·4
$\bar{C}(y)$	—	11·27	11·60	11·78	11·87	11·90	—	64·02	63·68	63·38	61·75
$S(y)$	—	0·48	0·54	0·39	0·38	0·40	—	1·16	0·77	0·71	2·04

$\bar{C}(y)$ = Mean value (in y direction parallel to phases boundaries).
$S(y)$ = Standard deviation.

(ZGB, Fig. 7(a)), boundaries separating alumina grains (AGB, Fig. 7(b)), and boundaries in the M phase (MGB, Fig. 7(c)). The concentration profiles indicate Ce and La segregation at both ZGB and AGB, whereas in the MGB only a marginal increase in Ce concentration was measured. Composition profiles measured across the CZ/M phase boundary (ZMPB, Fig. 8) revealed a maximum for the Ce concentration on the CZ side close to the ZMPB interface.

4 Discussion

4.1 Structure of interfaces

The principal features of microstructure which have developed in Ce–La-TZP/Al_2O_3 composite ceramics are a consequence of the segregation behaviour of Ce and La dopants and reactions of SiO_2 impurities with CeO_{2-x} ($0 < x < 0{\cdot}5$) and ZrO_2 matrix constituents.

The microstructure observed in CZA composite consists of pure Al_2O_3 particles (A) dispersed in the CeO_2-stabilized tetragonal ZrO_2 matrix (CZ) Both crystalline phases are in contact with a vitreous intergranular phase at triple grain junctions (TJs). Mutual solid solubility between Al_2O_3 and ZrO_2 and between Al_2O_3 and CeO_2 could not be detected at the 1 mol% level, in agreement with existing phase diagrams for the system ZrO_2–Al_2O_3–CeO_2 at 1400°C.[19] Although previous TEM investigations indicated the existence of a continuous vitreous intergranular phase of uniform thickness in Ce-TZP[6] in agreement with theoretical considerations,[20] indications are that in these zirconia/alumina composites at least some phase and grain boundaries exist without a distinct intergranular phase present. The observation of misfit dislocations in these interfaces indicate an essentially crystalline nature of such boundaries, though they act as sinks for certain solutes as is evidenced by the experimental segregation profiles.

Using the space charge concept it is predicted that the substitution of Zr^{4+} by divalent and trivalent cations at concentrations higher than that of the intrinsic point defects (i.e. O-vacancies) results in positively charged grain boundaries in Ce-TZP.[12] This implies that divalent and trivalent cations (having effective charge of -2 and -1, respectively, in the ZrO_2 lattice) segregate to the grain boundaries, but tetravalent cations do not. It is known that under certain conditions Ce is partially reduced to its trivalent state Ce^{3+}.[21] Since at temperatures $T > 1000$°C trivalent Ce^{3+} cations are sufficiently abundant to be the predominant charged species, a positive charge is induced on grain boundaries in

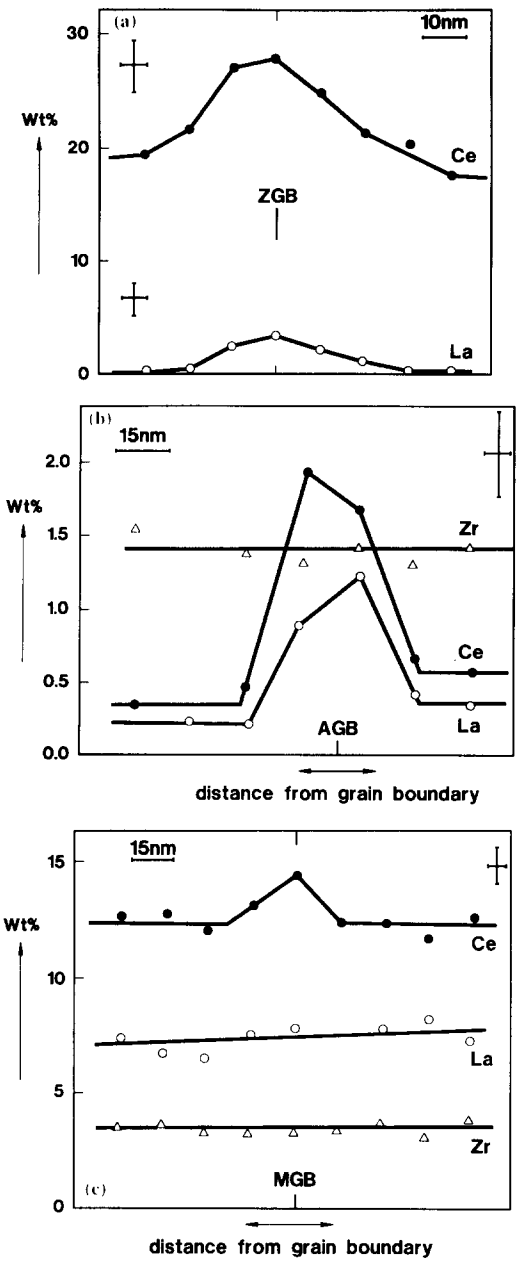

Fig. 7. Segregation on grain boundaries in composite CLZA: (a) Composition profiles across CZ matrix grain boundary (ZGB); (b) across alumina grain boundary (AGB); and (c) across grain boundary in the M phase (MGB).

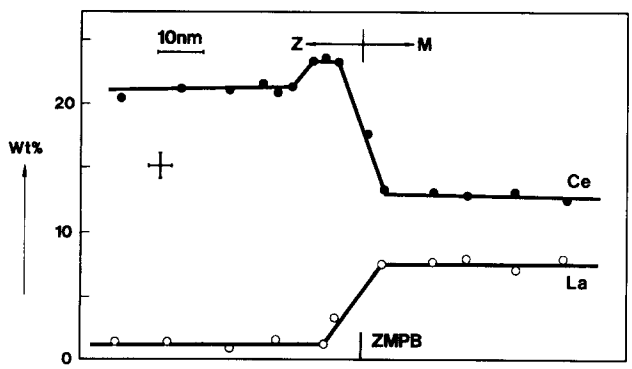

Fig. 8. Segregation on phase boundary in composite CLZA: Ce, La concentration profiles across the CZ/M phase boundary (ZMPB).

Ce-TZP. The observed Ce segregation on matrix grain boundaries (ZGB) would be compatible with this space charge model if a trivalent state is assumed for the Ce segregate.

This model is also consistent with the observation that although Si impurities are accumulating in second-phase pockets at triple grain junctions, no indication on grain boundary segregation of the tetravalent Si could be detected. Segregation on grain boundaries exerts a solute drag on the mobility of grain boundaries and thus suppresses grain growth. In contrast, SiO_2 impurities tend to react with the segregates to form vitreous intergranular phases, which provide rapid material transport paths and thus assist densification in the sintering process.

The space charge arises near any geometric discontinuity, including solid–liquid phase boundaries at wetted two-grain junctions. Thus, the segregation behaviour of wetted grain boundaries should not be principally different from that of 'clean' non-wetted interfaces. It is assumed that diffusion across the thin film of vitreous intergranular phase is fast compared to solute drag, which is controlled by lattice diffusion. Thus, the mobility of grain and phase boundaries, irrespective of being wetted by a thin film of intergranular phase can still be rate limited by the solute drag exerted by cations segregated to interface regions, as pointed out by Hwang & Chen.[12]

Under heterogeneous sampling conditions, as are encountered in EDS analysis in GB regions, the measured intensities of the X-ray signals are proportional to the convolution product of the electron density distribution function in the probe and the concentration distribution function and thus do not necessarily reflect the true concentrations in the volume sampled.[14] In the case of a thin intergranular film of thickness $\delta \ll D_{\text{eff}}$, where D_{eff} is the effective probe size (including beam broadening), the measured apparent concentrations can grossly underestimate the true concentrations in the GB phase because of a dilution effect by phase overlap due to contributions to the X-ray signal from the adjacent matrix grains. The experimentally measured composition profiles across grain boundaries showed full widths at half maximum (FWHM) in the order of 30 nm, thus exceeding the probe size approximately by an order of magnitude. Since the convolution product is dominated by the geometrically wider function, the authors believe that the measured profiles reflect true concentrations, at least in the case where a distinct secondary phase is absent. The width of measured segregation profiles

should thus be independent of the presence of a thin film of intergranular phase. However, cation concentrations in the GB phase in excess of segregate concentrations in GB regions, particularly Ce and Al, will result in excess apparent segregate concentrations on wetted grain boundaries.

Though grain boundaries in pure Al_2O_3 are reported to carry a positive charge,[22] the observed segregation of Ce, Zr and La on Al_2O_3 grain boundaries is not explicable by the space charge model, since tetravalent and isoelectric trivalent solutes in Al_2O_3 have effective charges of $+1$ and zero, respectively. It is argued that due to large differences in ionic radii the solute misfit strain energy is the dominating driving force for the segregation of Ce and La, and to a lesser extent for Zr on AGBs. On the other hand, a small misfit strain and thus a negligible tendency for grain boundary segregation would be expected for Si solute in Al_2O_3, in agreement with the present observations. A similar behaviour was reported for the segregation of Si, Zr and La solutes on grain boundaries in Al_2O_3, where ion misfit strain energy seems to be the driving force for segregation.[23]

Since the Al_2O_3 particles dispersed in Ce-TZP are observed to occupy predominantly intergranular positions, these particles exhibit a grain boundary pinning effect. If the kinetics of dissolution and reprecipitation of such particles are slower than the kinetics of grain growth in the matrix phase, the intergranular particles cannot retain their equilibrium positions in advancing grain boundaries, resulting in reduced grain growth in combination with solute drag. It has been reported that if growth rates of matrix grains are much higher than the dissolution and reprecipitation rates at the contact areas, small spherical inert second-phase particles detach from moving boundaries during Ostwald ripening of the matrix phase and become entrapped in matrix grains even in systems where thin vitreous intergranular films exist.[24] This has been confirmed by the authors' own experiments where occasionally small spherical Al_2O_3 particles entrapped inside Ce-TZP matrix grains have been observed.

4.2 Formation of M phase

The addition of 1 mol% La_2O_3 to the Ce-TZP/Al_2O_3 composite had a pronounced effect on phase interreaction and the resulting microstructure. The AEM experiments revealed a microstructure consisting of a pure CeO_2-stabilized t-ZrO_2 matrix phase (CZ) in coexistence with pure Al_2O_3 particles (A) and an Al–Ce–La–Zr mixed oxide phase (M). It should be noted that the experimentally measured La concentration in the matrix phase is $<0{\cdot}7\%$ (by wt), suggesting maximum solubility of La_2O_3 in ZrO_2 of the order of $\lesssim 0{\cdot}5$ mol% at room temperature, in agreement with literature reports.[25]

Electron diffraction experiments suggested that the M phase is isostructural with the magnetoplumbite-type (MP) compounds $La_2O_3 . 11Al_2O_3$ and $Ce_2O_3 . 11Al_2O_3$, with hexagonal symmetry and lattice parameters $a = 0{\cdot}555$ nm, $c = 2{\cdot}202$ nm.[26] Twenty EDS spectra have been collected on individual M grains and the results were statistically evaluated. The analysis revealed a highly homogeneous composition for the M phase, as indicated by the standard deviations, which are in the order of the expected measuring errors (Table 3). The cation ratio Al:Ce:La:Zr $\approx 93{\cdot}5:3{\cdot}5:2:1$ as measured in the M phase gives a ratio Al:(Ce + La + Zr) = 14·4 which is identical to the Al:La ratio in an Al-rich MP-type lanthanum hexaluminate with composition $La_{0{\cdot}827}Al_{11{\cdot}9}O_{19{\cdot}09}$ reported in the literature.[27] Earlier investigations on hexagonal rare earth aluminates confirmed that both trivalent Ce and La form stable phases.[26] However, studies on the kinetics of the latter phase formed via a two-stage process

$$La_2O_3 + Al_2O_3 \rightarrow 2LaAlO_3$$

$$LaAlO_3 + 5Al_2O_3 \rightarrow LaAl_{11}O_{18}$$

revealed an extremely slow solid-state kinetic at $T = 1450°C$ for the second reaction.[28] Since neither the $LaAlO_3$ nor the isostructural $Ce^{3+}AlO_3$ phase could be detected in this material it is argued that the M phase is either formed from Ce_2O_3 and La_2O_3 in a single-stage solid state reaction with Al_2O_3, or the kinetics of the substitution of coupled (Ce_2O_3 + La_2O_3) (plus some ZrO_2) in alumina are fast enough to be completed within the sintering time applied. Studies on the solid-state kinetics of $LaAl_{11}O_{18}$ suggested the availability of external oxygen as the rate-limiting factor for the formation of this compound via the two-stage solid-state reaction.[28] Since an abundance of Ce^{3+} indicates reducing conditions during the sintering process it is argued that the M phase may rather be formed by a coupled substitution process via a single-stage reaction. This view is further supported by a recent report[29] on a similar reaction in which the simultaneous additions of SrO and Al_2O_3 to 12Ce-TZP resulted in the in-situ formation of strontium hexaluminate ($SrO . 6Al_2O_3$).

It should be noted that the expected trivalent state for Ce in the M phase was indeed confirmed by precision measurements on the chemical shift of the Ce-$M_{4,5}$ ionization edges in electron energy-loss

spectra (EELS).[18] This observation thus lends further support to the assumption that the trivalent Ce and La cations segregate on positively charged grain boundaries and are eventually expelled from the zirconia lattice, driven by the coherency lattice strain in grain boundary regions.[21] As shown by the authors' experiments, Ce^{3+} does not react with Al_2O_3 on its own at $T = 1400°C$, thus the expelled Ce contributes to the formation of a vitreous intergranular phase as seen in composite CZA. In contrast, the formation of the M phase readily absorbed the trivalent Ce and La segregates, thus there is very little intergranular glassy phase formed in the composite CLZA, which results in lower densification. There is also an increased grain growth (1·7 μm versus 1 μm) during sintering in comparison with the CZA, due to the lower solute drag exerted by trivalent Ce and La species attracted to form the M phase.

The fact that the M phase is in coexistence with an unidentified (Ce, La)-rich phase (Fig. 5) suggests a narrow region in the Ce_2O_3–La_2O_3–Al_2O_3 system in which the M phase exists, and the percentages given in Table 4 are interpreted as the upper limits for Ce and La concentrations in the M phase. This view is supported by the experimentally measured composition gradients across M grains (Fig. 6(b)). The profiles reflect a high homogeneity in Ce and La concentrations, whereas the Zr content seems to be influenced by the CZ environment.

5 Summary and Conclusions

The comparison of the CZA and CLZA microstructures revealed the role of La in the phase-forming process within these composite materials.

In the composite CZA the grain boundary segregation of the Ce^{3+} controls the mean grain size (1 μm) and when expelled from the Ce-TZP lattice allows the reaction with SiO_2 impurities to form a glassy interface layer that enhances sinterability and density (98% th.). In the composite CLZA the presence of La^{3+} triggers the M phase formation which rapidly hosts both La^{3+} and Ce^{3+} cations segregated from the ZrO_2 matrix phase and thus prevents the glassy phase formation which results in a lower densification (96% th.) with larger mean grain size (1·7 μm).

These differences in microstructure are directly correlated to the resulting mechanical properties. The CZA composite presents a flexural strength of 600 MPa with intergranular fracture mode and a fracture toughness characterized by a K_{IC} of 12 MPa $m^{1/2}$, whereas the CLZA composite exhibits lower strength (500 MPa), transgranular fracture mode and increased fracture toughness to 15·5 MPa $m^{1/2}$.

References

1. Rühle, M., Claussen, N. & Heuer, A. H., Microstructural studies of Y_2O_3-containing tetragonal ZrO_2 polycrystals (Y-TZP). In *Advances in Ceramics, Vol. 12, Science and Technology of Zirconia II*, ed. N. Claussen, M. Rühle & A. H. Heuer. Am. Ceram. Soc., Columbus, OH, 1984, pp. 352–70.
2. Nettleship, I. & Stevens, R., Tetragonal zirconia polycrystals (TZP)—a review. *Int. J. High Technol. Ceram.*, **3** (1987) 1–32.
3. Hannink, R. H. J. & Swain, M. V., Metastability of the martensitic transformation in a 12 mol% ceria–zirconia alloy: I. Deformation and fracture observations. *J. Am. Ceram. Soc.*, **72** (1989) 90–8.
4. Nieh, T. G. & Wadworth, J., Superplastic behaviour of a fine-grained, yttria-stabilized tetragonal zirconia polycrystal (Y-TZP). *Acta Metall. Mater.*, **38** (1990) 1121–36.
5. Schmid, H. K., Microstructure of grain boundaries in ceramics. In *Proc. 1st Eur. Ceram. Soc. Conf.*, ed. G. de With, R. A. Terpstra & R. Metselaar. Elsevier Applied Science, London and NY, 1989, pp. 36–40.
6. Schmid, H. K., Microanalysis of grain boundary phases in Ce-TZP. *Inst. Phys. Conf. Ser., 93*, **2**(14) (1988) 539–40; Schmid, H. K. & Sonnenberg, N., Structure of interfaces in Ce-TZP. *Inst. Phys. Conf. Ser., 93*, **2**(14) (1988) 541–2.
7. Claussen, N., Microstructural design of zirconia-toughened ceramics (ZTC). In *Advances in Ceramics, Vol. 12, Science and Technology of Zirconia II*, ed. N. Claussen, M. Rühle & A. H. Heuer. Am. Ceram. Soc., Columbus, OH, 1984, pp. 325–51.
8. Evans, A. G., Perspective on the development of high-toughness ceramics. *J. Am. Ceram. Soc.*, **73** (1990) 187–206.
9. Tsukuma, K. & Ueda, K., Strength and fracture toughness of isostatically hot pressed composites of Al_2O_3 and Y_2O_3–partially-stabilized ZrO_2. *J. Am. Ceram. Soc.*, **68** (1985) C4–C5.
10. Tsukuma, K., Takahata, T. & Shiomi, M., Strength and fracture toughness of Y-TZP, Ce-TZP, Y-TZP/Al_2O_3 and Ce-TZP/Al_2O_3. In *Advances in Ceramics, Vol. 24, Science and Technology of Zirconia III*, Am. Ceram. Soc., Columbus, OH, 1988, pp. 721–30.
11. Schmid, C., Schubert, H. & Meriani, S., The role of alumina in zirconia–ceria composite alloys. In *Proc. 1st Eur. Ceram. Soc. Conf.*, ed. G. de With, R. A. Terpstra & R. Metselaar. Elsevier Applied Science, London and NY, 1989, pp. 547–53.
12. Hwang, S.-L. & Chen, I.-W., Grain size control of tetragonal zirconia polycrystals using the space charge concept. *J. Am. Ceram. Soc.*, **73** (1990) 3269–77.
13. Rühle, M., Evans, A. G., McMeeking, R. M. & Charlamides, P. G., Microcrack toughening in alumina/zirconia, *Acta Metall.*, **35** (1987) 2701–10.
14. Schmid, H. K., X-Ray microanalysis with high spatial resolution in the AEM. *Proc. Electr. Micr. Soc. South Africa*, **18** (1988) 35–6.
15. Bonnell, D. A., Rühle, M. & Tien, T.-Y., Redistributon of aluminum ions during processing of sialon ceramics. *J. Am. Ceram. Soc.*, **69** (1986) 623–7.
16. Schmid, H. K., Computer-assisted microanalysis in STEM. *Proc. Electr. Micr. Soc. South Africa*, **20** (1990) 7–8.

17. Schmid, H. K., Redistribution of Ce during processing of Si_3N_4/Ce-TZP and Ce-TZP/Al_2O_3 composites. In *Proc. 11th Risø Int. Symp. Metall. Mat. Sci., Structural Ceramics-Processing, Microstructure and Properties*, ed. J. J. Bentzen, J. B. Bilde-Sørensen, N. Christiansen, A. Horsewell & B. Ralph. Risø Nat. Lab. Roskilde, Denmark, 1990, pp. 483–8.
18. Schmid, H. K., EELS studies on the valency state of Ce, *Proc. Electr. Micr. Soc. South Afr.*, **21** (1991) 49–50.
19. Longo, V. & Podda, L., In *Phase diagrams for ceramists*, Vol. IV, Am. Ceram. Soc., Westerville, OH, Fig. 5437 (1981).
20. Clarke, D. R., On the equilibrium thickness of intergranular glass phases in ceramic materials. *J. Am. Ceram. Soc.*, **70** (1987) 15–22.
21. Schmid, H. K., Diffusion-induced grain-boundary migration in ceria-stabilized tetragonal zirconia polycrystals. *J. Am. Ceram. Soc.*, **74** (1991) 387–94.
22. Kingery, W. D., Plausible concepts necessary and sufficient for interpretation of ceramic grain-boundary phenomena: I. Grain-boundary characteristics, structure, and electrostatic potential. *J. Am. Ceram. Soc.*, **57** (1974) 1–8.
23. Li, C.-W. & Kingery, W. D., Solute segregation at grain boundaries in polycrystalline Al_2O_3 (structure and properties of MgO and Al_2O_2 ceramics, ed. W. D. Kingery), *Adv. in Ceram.*, **10** (1984) 368–78.
24. Kang, S.-J. L., Kaysser, W. A., Petzow, G. & Yoon, D. N., Growth of Mo grains around Al_2O_3 particles during liquid phase sintering. *Acta Metall.*, **33** (1985) 1919–26.
25. Bastide, B., Odier, P. & Coutures, J. P., Phase equilibrium and martensitic transformation in lanthana-doped zirconia. *J. Am. Ceram. Soc.*, **71** (1988) 449–53.
26. Liebertz, J., Rare-earth aluminate $SEAl_{11}O_{18}$, $SEMgAl_{11}O_{19}$ and $SELi_{0.5}Al_{11.5}O_{19}$. *Z. Kristallogr.*, **166** (1984) 297–300 (in German).
27. Inoue, N. I. Z., Takekawa, S. & Kimura, S., The crystal structure of lanthanum hexaaluminate. *J. Sol. State Chem.*, **54** (1984) 70–7.
28. Ropp, R. C. & Carroll, B., Solid-state kinetics of $LaAl_{11}O_{18}$. *J. Am. Ceram. Soc.*, **63** (1980) 416–19.
29. Cutler, R. A., Mayhew, R. J., Prettyman, K. M. & Virkar, A. V., High-toughness Ce-TZP/Al_2O_3 ceramics with improved hardness and strength. *J. Am. Ceram. Soc.*, **74** (1991) 179–86.